*Article*

# Persistence Length of PEGMA Bottle Brushes Determined by Pyrene Excimer Fluorescence

Janine L. Thoma [1], Hunter Little [1], Jean Duhamel [1,*], Lei Zhang [2] and Kam Tong Leung [2]

[1] Institute for Polymer Research, Waterloo Institute for Nanotechnology, Department of Chemistry, University of Waterloo, 200 University Avenue West, Waterloo, ON N2L 3G1, Canada; janine.thoma@empa.ch (J.L.T.); htlittle@uwaterloo.ca (H.L.)

[2] Waterloo Institute for Nanotechnology, Department of Chemistry, University of Waterloo, 200 University Avenue West, Waterloo, ON N2L 3G1, Canada; l38zhang@uwaterloo.ca (L.Z.); tong@uwaterloo.ca (K.T.L.)

[*] Correspondence: jduhamel@uwaterloo.ca

**Abstract:** Seven pyrene-labeled poly(oligo(ethylene glycol) methyl ether methacrylate)s (PyEG$_5$-PEG$_n$MAs) were prepared with $n$ = 0, 3, 4, 5, 7, 9, and 19 ethylene glycol units by copolymerizing a small amount of penta(ethylene glycol) 1-pyrenemethyl ether methacrylate with an EG$_n$MA monomer. The conformation of the PyEG$_5$-PEG$_n$MA polymers evolved from a random coil for PyEG$_5$-PEG$_0$MA or poly(methyl methacrylate) to a polymeric bottle brush (PBB) architecture with increasing side chain length. The fluorescence decays of the PyEG$_5$-PEG$_n$MA samples were fitted according to the fluorescence blob model (FBM) whose parameters were used, in combination with the Kratky–Porod equation, to calculate the persistence length of these polymers. The persistence lengths obtained from the PEF experiments were found to increase with the square of the number ($N_S$) of non-hydrogen atoms in the side chain as expected theoretically. The persistence lengths found with the PyEG$_5$-PEG$_n$MA samples in DMF also matched those found earlier for another series of PEG$_n$MA samples labeled with 1-pyrenebutanol. The good agreement found between the persistence lengths obtained with the PEG$_n$MA samples labeled with two different pyrene derivatives illustrates the robustness of the method and its applicability for measuring the unknown persistence length of polydisperse polymer samples.

**Keywords:** pyrene excimer fluorescence; persistence length; fluorescence blob model; Kratky–Porod equation

## 1. Introduction

The persistence length ($l_p$) is a core parameter in polymer science. In lay terms, $l_p$ reflects how easily a linear chain can bend, with $l_p$ decreasing with increasing chain flexibility. For instance, $l_p$ increases from 0.48 nm for flexible poly(ethylene oxide) [1] to 1.8 nm for more rigid bisphenol A polycarbonate [2]. Because stiffer polymers have a larger modulus ($G$), theoretical work has aimed to relate $l_p$ to $G$ to use $l_p$ for a given polymer as a predictor of the viscoelastic properties expected for its solution [3–7]. Computational methods yield $l_p$ by measuring the distance over which a vector tangent to the main chain loses its orientation as it is moved along the chain with respect to the tangent vector obtained at a reference point [8]. Experimentally, $l_p$ is measured by building conformational plots from measurements of the radius of gyration ($R_G$) [9,10] or the intrinsic viscosity ([$\eta$]) [11], obtained by scattering or viscosity experiments, respectively, as a function of the molecular weight of polymer samples prepared with a narrow molecular weight distribution (MWD). For many polymers, that cannot be produced with a narrow MWD, gel permeation chromatography (GPC) instruments equipped with a combination of differential refractive index, static light scattering, and viscosity detectors can be employed to generate conformation plots by taking advantage of GPC's ability to yield $R_G$ and [$\eta$] as a function of polymer molecular weight [12,13].

Despite its importance in polymer science, $l_p$ remains unknown for most polymers because many polymers cannot be obtained with a narrow MWD and require GPC analysis for $l_p$ determination. Unfortunately, GPC instruments are typically operated in a given solvent, which is not always suitable for all polymer types. Poorly soluble polymers induce interactions between the polymers and the packing material of the GPC column that result in distorted GPC traces, preventing the determination of $l_p$ by GPC analysis. Consequently, alternative experimental methods are required to determine $l_p$ for polydisperse polymer samples in solvents where they can be fully dissolved.

The interest in scattering or viscosity techniques for determining $l_p$ resides in their ability to use $R_G$ or $[\eta]$ to probe the local density generated inside the macromolecular volume defined by the polymer under study. Since a more flexible polymer can pack more structural units (SU) inside the same macromolecular volume occupied by a stiffer polymer, the polymer coil generated by the stiffer polymer is less dense than the polymer coil generated by the more flexible polymer, thus enabling the determination of $l_p$ from conformation plots established with $R_G$ or $[\eta]$. This discussion suggests that in theory, any technique capable of probing the local density of a polymer coil in solution should be able to yield $l_p$ for that polymer.

One such technique was recently presented using a methodology based on pyrene excimer formation (PEF) between an excited and a ground-state pyrenyl label covalently attached to a macromolecule. Since PEF is a chemical reaction, its efficiency depends on the local concentration ($[Py]_{loc}$) of ground-state pyrenes found within the macromolecular volume [14]. This dependency was recently established by demonstrating that the average rate constant ($<k>$) for PEF between pyrenyl labels attached to a macromolecule is directly proportional to $[Py]_{loc}$ [15]. Since the experimentalist knows where the pyrenyl labels are attached on the pyrene-labeled macromolecule (PyLM), $[Py]_{loc}$ reflects the local density of a PyLM, thus enabling the application of PEF to determine $l_p$. The PEF-based methodology that was developed to determine $l_p$ uses polymers that were randomly labeled with pyrene and whose fluorescence decays were fitted according to the fluorescence *blob* model (FBM) [16]. Within the framework of the FBM, an excited pyrenyl label only probes a subvolume, also referred to as a *blob*, of the much larger polymer coil. The *blob* is then used as a unit volume to compartmentalize the polymer coil into a cluster of *blobs* among which the pyrenyl labels distribute themselves randomly with a Poisson distribution. As for any *blob*-based method, the use of *blobs* shifts the study from the entire polymer to that of a *blob*, eliminating problems associated with polydisperse samples, that often plague scattering studies [17,18] since a large or small polymer can be described by many or few identical *blobs* [19]. The FBM analysis of the fluorescence decays yields the average number $<n>$ of pyrenyl groups per *blob*, which is used to determine the number $N_{blob}$ of SU per *blob*. Since a flexible polymer can pack more SU inside a *blob* than a stiffer polymer, $N_{blob}$ is larger for a flexible polymer than for a stiffer polymer and thus responds to $l_p$.

With this insight, the dependency of $N_{blob}$ on the flexibility, and thus $l_p$, of a polymer was recently taken advantage of to determine $l_p$ for a series of poly(oligo(ethylene glycol) methyl ether methacrylate)s, that were labeled with a 1-pyrenebutyl derivative and are referred to as PyBut-PEG$_n$MA [20]. However, only $l_p$ values that are smaller than the dimension of a *blob* probed by an excited pyrenyl label, can be measured with sufficient accuracy. Since the polymer backbone is much less mobile than the pyrenyl label, the linker connecting the pyrene moiety to the polymer backbone defines the size of the *blob*, which can be viewed as a sphere with an equivalent diameter of 3.0 nm in the case of the 1-pyrenebutyl derivative [20]. This meant that $l_p$ no greater than 2.0 nm could be measured with the PyBut-PEG$_n$MA samples [20]. While a range of $l_p$ values up to 2.0 nm covers a sizeable group of polymers that can be as flexible as PEO with an $l_p$ of 0.48 nm [1], to bisphenol A polycarbonate with an $l_p$ of 1.8 nm [2], the ability to determine an $l_p$ larger than 2.0 nm would enable the study of stiffer backbones. With this in mind, this report describes how labeling PEG$_n$MA with a 1-pyrenemethoxy-penta(ethylene glycol) derivative to yield PyEG$_5$-PEG$_n$MA samples enlarged the diameter of a *blob* from 3.0 nm for the PyBut-

PEG$_n$MA samples to 5.4 nm in *N,N*-dimethylformamide, thus enabling the measurement of $l_p$ values of up to 4.0 nm. The increase in $l_p$ values recovered with the PyEG$_5$-PEG$_n$MA samples from 2.0 to 4.0 nm represents a significant improvement in the range of $l_p$ values that can be determined from this PEF-based method and it will enable the study of stiffer polymer backbones.

## 2. Materials and Methods

### 2.1. Materials

Copper(II) bromide (Sigma, St Louis, MI, USA, 99%), Celite (Sigma), dichloromethane (DCM, Sigma, $\geq$99.8%), diethylether (Sigma, $\geq$99%), *N,N*-dimethylformamide (DMF, Sigma, $\geq$99.8%), dimethyl sulfoxide (DMSO, Sigma, $\geq$99.9%), 4-(dimethylamino)pyridine (DMAP, Sigma, $\geq$99%), ethyl acetate (Sigma, $\geq$99.7%), ethyl-$\alpha$-bromoisobutyrate (Sigma, 98%), tetra(ethylene glycol) methyl ether (EG$_4$, PurePEG, San Diego, CA, USA, $\geq$97%), penta(ethylene glycol) (Fisher, Hampton, NJ, USA, $\geq$95%), penta(ethylene glycol) methyl ether (EG$_5$, PurePEG, $\geq$95%), hepta(ethylene glycol) methyl ether (EG$_7$, TCI, Portland, OR, USA, $\geq$97%), 1,1,4,7,10,10-hexamethyl-triethylenetetramine (HMTETA, Sigma, $\geq$97%), methacrylic anhydride (Sigma, 94%), 1-pyrenemethanol (Sigma, 98%), sodium chloride (Sigma), sodium hydride (NaH, Sigma, 60% dispersion in mineral oil), sodium hydroxide (NaOH, Sigma, pellets, $\geq$97%), sodium sulfate (Sigma, anhydrous, $\geq$99%), tetrahydrofuran (Sigma, $\geq$99%), tetrahydrofuran optima (Fisher, $\geq$99.9%), and triethylamine (Sigma, $\geq$99.5%) were used as received.

Tri(ethylene glycol) methyl ether methacrylate (EG$_3$MA, Sigma, 93%) and two oligo(ethylene glycol) methyl ether methacrylates (EG$_9$MA with number average molecular weight ($M_n$) = 500 g/mol and EG$_{19}$MA with $M_n$ = 950 g/mol, Sigma) were dissolved in DCM, washed with 2 M NaOH, and dried with sodium sulfate before use. The radical initiator 2,2′-azo-*bis*-isobutyronitrile (AIBN, Sigma, 98%) was recrystallized in ethanol three times. *p*-Toluenesulfonyl chloride (Sigma, $\geq$98%) was dissolved in diethyl ether and washed with 2 M NaOH. The organic phase was extracted and dried with sodium sulfate. Unless otherwise specified, all other chemicals were purchased from commercially available sources and used as received.

### 2.2. Preparation of Penta(Ethylene Glycol) Mono p-Toluene Sulfonate (Tos$_1$-EG$_5$OH)

Penta(ethylene glycol) (EG$_5$) (2.00 g, 8.39 mmol) was added to a round bottom flask (RBF) equipped with a magnetic stirrer with freshly distilled DCM. Re-crystallized *p*-toluenesulfonyl chloride (1.76 g, 9.23 mmol) and triethyl amine (1.74 mL, 12.6 mmol) were added to the RBF and left to stir overnight. The next day, the reaction mixture was washed three times with a saturated solution of aqueous sodium chloride. The organic layer was extracted and dried with sodium sulfate. Silica gel chromatography was used to purify the singly tosylated EG$_5$ (Tos$_1$-EG$_5$OH) from the doubly tosylated EG$_5$ and unmodified EG$_5$ using ethyl acetate as the eluent. The Tos$_1$-EG$_5$OH fraction was dried in vacuo (vacuum oven from VWR, Radnor, PA, USA) and its chemical composition was verified using $^1$H NMR (Figure S1 in SI).

### 2.3. Preparation of 1-Pyrenemethyl Ether Penta(Ethylene Glycol) (PyEG$_5$OH)

1-Pyrenemethanol (1.18 g, 5.10 mmol) was added to a RBF with 50 mL of dried and distilled DMF. The solution was stirred and kept under a nitrogen atmosphere. Sodium hydride (NaH) (0.20 g, 5.10 mmol) was added to the RBF and the solution was allowed to stir for 1 h during which time the color of the solution changed from yellow to dark red/purple. Tos$_1$-EG$_5$OH (1.00 g, 2.55 mmol) was then added. The RBF was placed in an oil bath at 55 °C and left to stir overnight. After the RBF was removed from the oil bath and allowed to cool, 5 mL of Milli-Q water was added to the reaction solution to quench any unreacted NaH. Milli-Q water (50 mL) was then added to the reaction mixture, which was washed with 50 mL of ethyl acetate. The organic phase was collected and dried with sodium sulfate. The crude product was purified by silica gel chromatography using ethyl

acetate as the eluent. The chemical composition of the purified $PyEG_5OH$ product was confirmed using $^1H$ NMR (Figure S2 in SI).

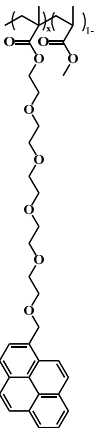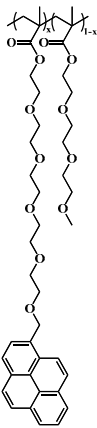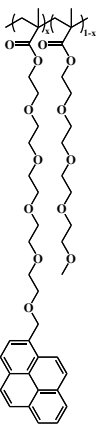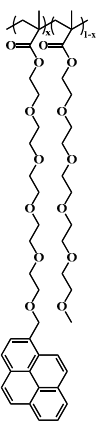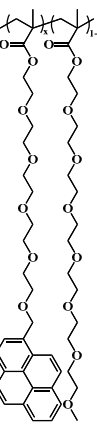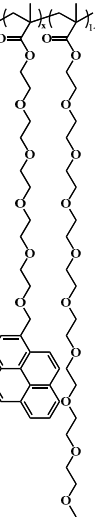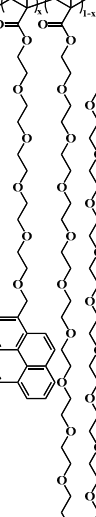### 2.4. Methacrylation of Oligo(Ethylene Glycol) Methyl Ethers ($EG_nOHs$) and $PyEG_5OH$

The same protocol was used to prepare the methacrylated oligo(ethylene glycol) methyl ethers ($EG_nMAs$, where $n$ = 4, 5, 7) and $PyEG_5MA$. The synthesis of $EG_5MA$ is described in more detail hereafter.

$EG_5OH$ (2.00 g, 7.93 mmol) and DMAP (0.0968 g, 0.793 mmol) were added to a RBF with 25 mL of freshly distilled DCM. The RBF was then placed in an ice water bath and the solution was stirred as methacrylic anhydride was added dropwise (1.18 mL, 7.93 mmol). The reaction was left to stir overnight. The reaction mixture was then washed three times with 2 M NaOH. The organic phase was extracted and dried with sodium sulfate. The crude product was purified by silica gel chromatography using ethyl acetate as the eluent. The chemical composition of the purified $EG_5MA$ macromonomer was characterized by $^1H$ NMR (Figure S3 in SI).

### 2.5. Random Copolymerization Using Conventional Radical Polymerization

The pyrene-labeled poly(oligo(ethylene glycol) methyl ether methacrylate)s ($PyEG_5$-$PEG_nMA$) were prepared by conventional radical polymerization of methyl methacrylate ($EG_0MA$), tri(ethylene glycol) methyl ether methacrylate ($EG_3MA$), tetra(ethylene glycol) methyl ether methacrylate ($EG_4MA$), penta(ethylene glycol) methyl ether methacrylate ($EG_5MA$), hepta(ethylene glycol) methyl ether methacrylate ($EG_7MA$), and two oligo(ethylene glycol) methyl ether methacrylates ($EG_9MA$ and $EG_{19}MA$) with $PyEG_5MA$. The chemical structure of the $PyEG_5$-$PEG_nMA$ samples is shown in Table 1. The moles of $PyEG_5MA$ used in the polymerization were varied to obtain different molar percentages of pyrene-labeling, ranging from 1 to 10 mol % of $PyEG_5MA$, incorporated into the $PyEG_5$-$PEG_nMA$ samples. The polymerization of $PyEG_5$-$PEG_0MA$ labeled with 2 mol % of $PyEG_5MA$ is described in more detail hereafter.

**Table 1.** Chemical structure of the $PyEG_5$-$PEG_nMA$ samples with the number of atoms ($N_S$) in each side chain and the molecular weight of the structural unit ($MW$(SU)).

| Sample | $PyEG_5$-$PEG_0MA$ | $PyEG_5$-$PEG_3MA$ | $PyEG_5$-$PEG_4MA$ | $PyEG_5$-$PEG_5MA$ | $PyEG_5$-$PEG_7MA$ | $PyEG_5$-$PEG_9MA$ | $PyEG_5$-$PEG_{19}MA$ |
|---|---|---|---|---|---|---|---|
| Structure |  | | | | | | |
| $N_S$ | 3 | 12 | 15 | 18 | 24 | 30 | 60 |
| $MW$(SU) g/mol | 100 | 232 | 276 | 320 | 408 | 500 | 950 |

PyEG$_5$MA (0.02 g, 0.04 mmol) and methyl methacrylate (EG$_0$MA, 0.20 g, 2.00 mmol) were dissolved in 6.8 mL of THF such that the overall methacrylate concentration was approximately 0.3 M. The AIBN initiator (2.00 µg, 0.01 µmol) was added to the monomer solution from a stock solution and the mixture was placed in the polymerization tube. The tube was kept on ice before being degassed with nitrogen (Praxair, Danburry, CT, USA, N4.0) for 30 min. After sealing the tube, it was left in an oil bath at 65 °C. The polymerization was terminated after a conversion of 20% or less was reached, as determined by $^1$H NMR analysis, to minimize an eventual composition drift. The polymer was recovered by precipitating 5–6 times the polymer solution in THF into diethyl ether to remove any unreacted monomer. The precipitated product was then dried in a vacuum oven overnight at room temperature.

### 2.6. Random Copolymerization Using Initiators for Continuous Activator Regeneration Atom Transfer Radical Polymerization (ICAR-ATRP)

Three of the PyEG$_5$-PEG$_{19}$MA samples were prepared using ICAR-ATRP [21]. The protocol described for free radical copolymerization was applied to prepare PyEG$_5$-PEG$_{19}$MA using ethyl-$\alpha$-bromoisobutyrate, Cu(II)Br/HMTETA, and AIBN as initiator, catalyst/ligand system, and radical source, respectively. An example of the ICAR-ATRP of PyEG$_5$-PEG$_{19}$MA is provided in more detail hereafter.

A solution of PyEG$_5$MA (0.02 g, 0.04 mmol) and EG$_{19}$MA (1.00 g, 1.05 mmol) in 3.6 mL of THF, where the overall methacrylate concentration equaled 0.3 M, was transferred to the polymerization tube. A stock solution of Cu(II)Br (1.18 mg, 5.28 µmol) and HMTETA (4.3 µL, 15.8 µmol) was prepared in 10 mL of THF from which 10 µL was added to the polymerization tube. Ethyl-$\alpha$-bromoisobutyrate (10.0 µL, 68.1 µmol) was added to 1 mL of THF from which 7.8 µL was added to the polymerization tube. AIBN (5.00 mg, 0.03 mmol) was added to 10 mL of THF to make a 3.05 mM stock solution. The solution was further diluted to 0.3 mM from which 0.2 mL was added to the polymerization tube, which was placed on ice and degassed for 30 min with nitrogen (Praxair, N4.0). The tube was then sealed and heated to 60 °C in an oil bath for 20 h. Before the polymer was precipitated, the polymer solution in THF was filtered through a silica gel and Celite plug three times to remove copper. The polymer was further purified by 5–6 precipitations into diethyl ether.

### 2.7. Chemical Composition and Molecular Weight Distribution

The chemical composition of the PyEG$_5$-PEG$_n$MA polymers was confirmed by the analysis of the $^1$H NMR spectra acquired on a Bruker 300 MHz high resolution spectrometer (Bruker, Billerica, MA, USA). A sample $^1$H NMR spectrum of PyEG$_5$-PEG$_5$MA is provided in Figure S4 in the SI. The molecular weight distribution (MWD) of each PyEG$_5$-PEG$_n$MA sample was determined by GPC analysis using either THF or DMSO. The pyrene contents (in mol%), $M_n$, and dispersity (Đ) of each sample are listed in Table 2.

**Table 2.** Pyrene content, absolute $M_n$, and dispersity of the PyEG$_5$-PEG$_n$MA samples.

| PyEG$_5$-PEG$_0$MA | | | PyEG$_5$-PEG$_3$MA | | | PyEG$_5$-PEG$_4$MA | | |
|---|---|---|---|---|---|---|---|---|
| Pyrene Content (mol%) | $M_n$ (g/mol) [a] | Đ | Pyrene Content (mol%) | $M_n$ (g/mol) [a] | Đ | Pyrene Content (mol%) | $M_n$ (g/mol) [a] | Đ |
| 0.9 | 40,000 | 1.6 | 0 | 293,000 | 2.9 | 1.2 | 105,000 | 1.5 |
| 2.0 | 45,000 | 1.3 | 0.5 | 153,000 | 2.7 | 1.9 | 84,000 | 1.6 |
| 2.6 | 24,000 | 1.3 | 1.6 | 118,000 | 1.9 | 2.2 | 88,000 | 1.5 |
| 3.3 | 43,000 | 1.8 | 2.0 | 128,000 | 2.8 | 2.4 | 83,000 | 1.4 |
| 3.3 | 46,000 | 1.5 | 2.0 | 149,000 | 3.0 | 3.1 | 89,000 | 1.3 |
| - | - | - | 3.0 | 200,000 | 1.7 | - | - | - |
| - | - | - | 3.4 | 91,000 | 2.1 | - | - | - |
| - | - | - | 3.8 | 150,000 | 1.6 | - | - | - |

**Table 2.** *Cont.*

| PyEG$_5$-PEG$_5$MA | | | PyEG$_5$-PEG$_7$MA | | | PyEG$_5$-PEG$_9$MA | | |
|---|---|---|---|---|---|---|---|---|
| Pyrene Content (mol%) | $M_n$ (g/mol) [b] | Đ | Pyrene Content (mol%) | $M_n$ (g/mol) [b] | Đ | Pyrene Content (mol%) | $M_n$ (g/mol) [b] | Đ |
| 0.4 | 121,000 | 2.1 | 2.2 | 232,200 | 3.8 | 0 | 152,000 | 1.5 |
| 2.2 | 55,000 | 1.6 | 3.0 | 222,000 | 3.7 | 0.8 | 420,000 | 3.4 |
| 3.6 | 95,000 | 2.0 | 3.6 | 304,000 | 3.5 | 2.9 | 257,000 | 1.5 |
| 3.8 | 86,000 | 1.7 | 4.2 | 109,000 | 1.8 | 5.2 | 166,000 | 1.6 |
| 4.8 | 106,000 | 2.3 | - | - | - | 5.8 | 154,000 | 1.3 |
| 6.5 | 64,000 | 1.5 | - | - | - | 7.4 | 173,000 | 1.4 |
| - | - | - | - | - | - | 10.2 | 186,000 | 1.6 |

| PyEG$_5$-PEG$_{19}$MA | | |
|---|---|---|
| Pyrene Content (mol%) | $M_n$ (g/mol) [b] | Đ |
| 0 | 134,000 | 1.4 |
| 0.9 | 187,000 | 1.2 |
| 2.1 | 194,000 | 1.3 |
| 3.2 | 683,000 | 2.8 |
| 4.1 | 132,000 | 2.1 |
| 5.2 | 85,300 | 1.3 |
| 6.2 | 274,000 | 1.5 |
| 6.6 | 92,000 | 1.3 |

[a] GPC in THF. [b] GPC in DMSO.

### 2.8. Pyrene Content of PyEG$_5$-PEG$_n$MA Samples

The pyrene content expressed as the molar fraction ($x$) of the PyEG$_5$MA monomer incorporated in the copolymers, equivalent to the molar fraction of structural units bearing a pyrenyl labels, was calculated with Equation (1).

$$x = \frac{M}{\lambda_{Py}^{-1} + M - M_{Py}} \tag{1}$$

In Equation (1), $\lambda_{Py}$, $M$, and $M_{Py}$ are the pyrene content of the polymer expressed in mol of pyrene per gram of polymer and the molar mass of the EG$_n$MA and PyEG$_5$MA monomers, respectively. $\lambda_{Py}$ was determined as follows. A polymer solution was prepared in THF with a known mass concentration ($m$) of a PyEG$_5$-PEG$_n$MA sample. The pyrene content of the polymer ($\lambda_{Py}$) was calculated from the ratio $Abs/(m \times \varepsilon)$, where $Abs$ is the absorption at 344 nm of the PyEG$_5$-PEG$_n$MA solution in THF and $\varepsilon$ is the molar absorption coefficient of 1-pyrenemethanol in THF ($\varepsilon$(344 nm) = 42,700 M$^{-1}\cdot$cm$^{-1}$) [22].

### 2.9. Gel Permeation Chromatography (GPC)

Absolute molecular weights were obtained for PyEG$_5$-PEG$_0$MA, PyEG$_5$-PEG$_3$MA, and PyEG$_5$-PEG$_5$MA by injecting 1 mg/mL solutions of the samples dissolved in THF into a Viscotek GPC (Viscotek, Houston, TX, USA) equipped with a differential refractive index, static light scattering (low and right angle), and UV–Vis absorption detector and three 300 × 8 mm$^2$ PolyAnalytik Superes linear mixed-bed columns (PolyAnalytik, London, ON, Canada). A flow rate of 1 mL/min of THF at 35 °C was used. The system was calibrated with a 1 mg/mL THF solution of a polystyrene (PS) standard with $M = 90 \times 10^3$ g·mol$^{-1}$ and Đ = 1.04.

However, PyEG$_5$-PEG$_7$MA, PyEG$_5$-PEG$_9$MA, and PyEG$_5$-PEG$_{19}$MA were found to interact with the column set of the GPC instrument in THF resulting in distorted GPC traces. As a result, the absolute molecular weights of these samples were obtained by injecting 2 mg/mL polymer solutions in DMSO into a TOSOH EcoSEC High Temperature GPC instrument equipped with a triple detection system and two 300 × 7.8 mm$^2$ TOSOH TSKgel Alpha-M 13 μm columns (Tosoh, Tokyo, Japan). This detection system included an in-line differential refractometer, a Wyatt Dawn Heleos8 MALLS detector (wavelength, λ = 660 nm) (Wyatt, Santa Barbara, CA, USA), and a viscometer. A flow rate of 0.6 mL/min of DMSO at 60 °C was used. The system was calibrated with a 1 mg/mL solution of pullulan standard in DMSO with $M_w = 47.1 \times 10^3$ g·mol$^{-1}$ and *Đ* = 1.07.

The specific refractive index increment (*d*n/*d*c) of each polymer in THF and DMSO was calculated using the differential refractometers of the GPC instruments. Sample GPC traces can be found in Figure S5 in SI.

### 2.10. Atomic Force Microscopy (AFM)

AFM images were obtained with a Digital Instruments Dimension 3100 AFM (Digital Instruments, Santa Barbara, CA, USA) at room temperature using a silicon cantilever in the tapping mode. The samples were prepared by spin coating a few drops of a dilute solution of polymer dissolved in tetrahydrofuran (THF) (10 mg/L) onto a freshly cleaved mica surface at 2000 rpm.

### 2.11. UV–Vis Spectroscopy

A Varian Cary 100 Bio spectrophotometer (Varian, Palo Alto, CA, USA) was used to acquire the absorption spectra of the polymer solutions.

### 2.12. Steady-State Fluorescence (SSF) Measurements

All fluorescence spectra were acquired on a Horiba QM-400 spectrofluorometer equipped with a Xenon arc lamp (HORIBA Canada, Burlington, ON, Canada). The SSF spectra were acquired for polymer solutions in aerated DMSO with a $2.5 \times 10^{-6}$ M pyrene concentration equivalent to an absorbance of ~0.1 at 344 nm. The solutions were excited at 344 nm and scanned from 350 to 600 nm using 1 nm slit widths for both the excitation and emission monochromator. Dividing the florescence intensity of the excimer ($I_E$) by the fluorescence intensity of the monomer ($I_M$), calculated by integrating the area underneath the spectrum from 500 to 510 nm and from 375 to 381 nm, respectively, yielded the $I_E/I_M$ ratio, which was used to quantify the efficiency of pyrene excimer formation (PEF).

### 2.13. Time Resolved Fluorescence (TRF) Measurements

All fluorescence decays were obtained with an IBH time-resolved fluorometer (IBH, Glasgow, SCT, UK). The solutions were excited at 344 nm and the monomer and excimer fluorescence decays were acquired with 20,000 counts at the decay maximum over 1024 channels at 375 and 510 nm using cut-off filters at 370 and 495 nm, respectively. A time-per-channel of either 1.02 ns/ch or 2.04 ns/ch was employed for the decay acquisition. A Ludox solution was used for the instrument response function (IRF), which was obtained by setting the emission monochromator at 344 nm. The IRF was convoluted with the FBM equations shown as Equations (S1) and (S2) in SI and the convolution result was compared to the experimental decay.

### 2.14. The Fluorescence Blob Model (FBM) Analysis

The FBM compartmentalizes a polymer into equally sized *blobs*, where the volume of a *blob* is the volume probed by a pyrenyl label, while it remains excited [14,16]. The four pyrene species $Py_{diff}$*, $Py_{k2}$*, $Py_{agg}$*, and $Py_{free}$* are considered to represent PEF, which occurs via a dynamic and static pathway. Dynamic PEF takes place sequentially. $Py_{diff}$* represents an excited pyrenyl group, whose diffusion in solution is controlled by the polymer backbone and side chain dynamics. $Py_{diff}$* diffuses inside a *blob* populated by other

ground-state pyrenes until $Py_{diff}*$ becomes close enough to a ground-state pyrene molecule for $Py_{diff}*$ to turn into $Py_{k2}*$. The diffusive motions of two pyrenyl groups inside a *blob* are described by the rate constant $k_{blob}$. Rapid rearrangement of $Py_{k2}*$ and the nearby ground-state pyrene with the large rate constant $k_2$ ($k_2 \sim 10 \times k_{blob}$) results in the formation of an excimer made of two pyrenyl labels, that are well ($E0*$), or poorly ($D*$) stacked and emit with their natural lifetimes $\tau_{E0}$ and $\tau_D$, respectively. Static PEF occurs through direct excitation of a pyrene aggregate resulting in the instantaneous formation of the $E0*$ or $D*$ species. The species $Py_{agg}*$ combines the two pyrenyl species $E0*$ and $D*$ formed instantaneously from the direct excitation of a pyrene aggregate. Finally, those excited pyrenes, that are isolated along the polymer backbone, do not form excimers, and emit with their natural lifetime $\tau_M$, and are referred to as $Py_{free}*$. During the decay analysis, the decays are fit twice, initially with a floating $k_2$ using the program *globmis90lbg* for all samples of a same $PyEG_5$-$PEG_nMA$ series prepared with different pyrene contents. All $k_2$ values obtained for a same polymer series are then averaged and the averaged $k_2$ value is then fixed in a second analysis with the program *globmis90obg*. The parameters retrieved from the FBM analysis with a fixed $k_2$ have much lower error bars. The molar fractions $f_{Mdiff}, f_{Mk2}, f_{Mfree}$, where the index $M$ indicates that they were derived from the monomer decays, and $f_{Ek2}, f_{EdiffE0}, f_{EE0}, f_{EdiffD}$, and $f_{ED}$, where the index $E$ indicates that they were derived from the excimer decays, were combined to yield the molar fractions $f_{diff}$ ($= f_{diffE0} + f_{diffD}$), $f_{k2}, f_{agg}$ ($= f_{E0} + f_D$), and $f_{free}$ for the pyrene species $Py_{diff}*, Py_{k2}*, Py_{agg}*$, and $Py_{free}*$, respectively. The average number ($<n>$) of ground state pyrene molecules inside a *blob* and the rate constant ($k_{blob}$) describing the diffusive encounters of two structural units bearing a pyrenyl label inside a *blob* were also obtained from the FBM analysis. The number ($N_{blob}$) of structural units encompassed within a *blob* was calculated using $f_{Mfree}$, $<n>$, and $x$ according to Equation (2).

$$N_{blob} = \frac{(1 - f_{M_{free}}) \times \langle n \rangle}{x} \tag{2}$$

Each pair of monomer and excimer fluorescence decays acquired for a given $PyEG_5$-$PEG_nMA$ sample was fit globally with Equations (S1) and (S2) in SI according to the FBM. The functions described by Equations (S1) and (S2) were convoluted with the IRF and the convolution product was compared to the experimental decays for optimization of the parameters with the Marquardt–Levenberg algorithm [23]. A fit was deemed acceptable when the $\chi^2$ was lower than 1.3 and when both the residuals and autocorrelation of the residuals were randomly distributed around zero.

### 2.15. Flow Chart Depicting the Methodology Applied for Determining the Persistence Length

The strategy applied to determine the persistence length by PEF is depicted in Figures 1 and 2. Figure 1 represents the experimental process to determine $<N_{blob}>$ for each $PyEG_5$-$PEG_nMA$ series and $N_{blob}^\infty$, which is the $<N_{blob}>$ value obtained for a hypothetical $PyEG_5$-$PEG_nMA$ sample having an infinitely long side chain ($n \to \infty$). Figure 2 is a geometrical construction describing the mathematical process applied to determine $l_p$ from $<N_{blob}>$ according to the Kratky–Porod equation [24]. In Figure 1, the fluorescence decays of the pyrene monomer and excimer shown in the left panel are acquired and fitted globally according to the FBM illustrated in the middle panel to determine $N_{blob}$ for different $PyEG_5$-$PEG_nMA$ samples of a same series with $n$ = 0, 3, 4, 5, 7, 9, and 19. The $N_{blob}$ values obtained for several pyrene contents of a same $PyEG_5$-$PEG_nMA$ series are averaged to obtain $<N_{blob}>$. These $<N_{blob}>$ values are plotted as a function of the molecular weight of a structural unit ($MW(SU)$) in the right panel of Figure 1. For small $MW(SU)$, $N_{blob}$ is large indicating a coiled conformation reflecting a small $l_p$. As $MW(SU)$ increases, $N_{blob}$ decreases as the chain conformation changes from a coiled to a worm-like conformation. For very large $MW(SU)$, the polymer chain achieves an extended conformation on the length-scale of the *blob*, $N_{blob}$ does not change any more with increasing $MW(SU)$, and its value corresponds to that expected for an extended polymer with infinitely long side chains ($N_{blob}^\infty$).
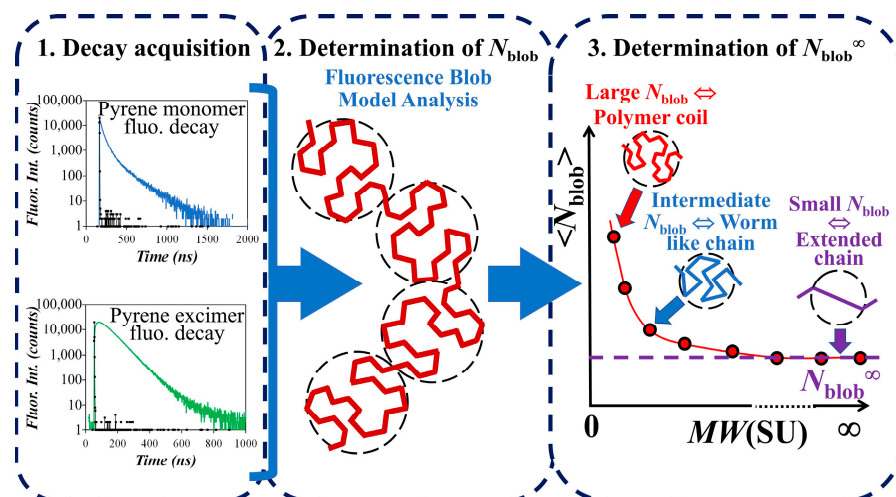
**Figure 1.** Depiction of the experimental process applied to determine $<N_{blob}>$ and $N_{blob}^{\infty}$ used to retrieve $l_p$.



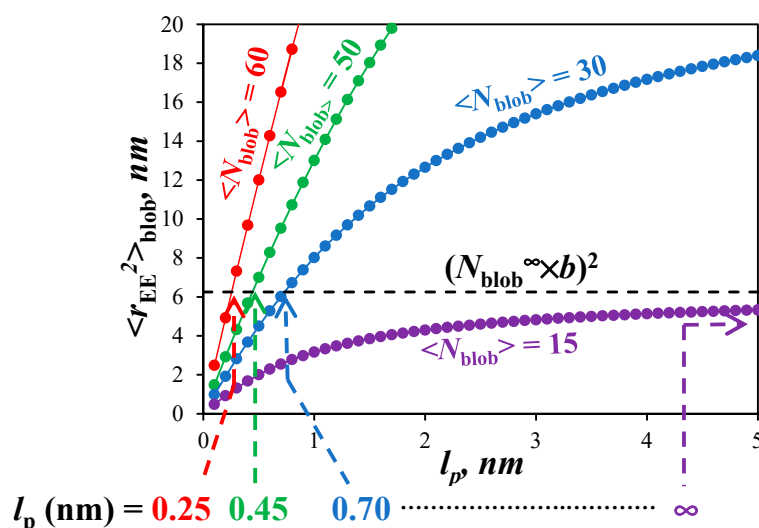**Figure 2.** Geometric construction depicting the mathematical procedure applied to retrieve $l_p$ from $<N_{blob}>$ and $N_{blob}^{\infty}$ determined in Figure 1.

Once $<N_{blob}>$ and $N_{blob}^{\infty}$ are determined, their values are introduced into Equation (3), which is a modified version of the Kratky–Porod equation (KPE) for worm-like chains to account for the fact that it is applied to the chain segment inside a *blob* instead of the entire chain. The left part of the KPE in Equation (3) represents the square of the end-to-end distance ($<r_{EE}^2>_{blob}$) of the chain fragment encompassed inside a *blob*. Since the pyrene moiety is connected to the polymethacrylate backbone with the same linker for all PyEG$_5$-PEG$_n$MA constructs, all PyEG$_5$-PEG$_n$MA samples share a same *blob* regardless of side chain length. According to this reasoning, $<r_{EE}^2>_{blob}$ takes the same value for all PyEG$_5$-PEG$_n$MA samples including those samples that have an infinitely long side chain for which the polymethacrylate backbone is fully extended. The fully extended polymethacrylate backbone corresponds to a hypothetical PyEG$_5$-PEG$_n$MA sample, for which $n$ and $MW(SU)$ take infinitely large values and $N_{blob}$ tends to $N_{blob}^{\infty}$ as shown in the right panel of Figure 1. For a fully extended chain segment inside a *blob*, $<r_{EE}^2>_{blob}$ equals the product $(N_{blob}^{\infty} \times b)^2$, where $b$ is the length of a methacrylate structural unit equal to 0.25 nm [25,26]. Since all PyEG$_5$-PEG$_n$MA share the same *blob* with $<r_{EE}^2>_{blob} = (N_{blob}^{\infty} \times b)^2$, the left-hand side of the KPE is known and the function on the right-hand side of the equation can be solved for $l_p$ as represented in Figure 2. The $<N_{blob}>$ value obtained for each PyEG$_5$-PEG$_n$MA series is entered into the right-hand side of the KPE, which is plotted as a

function of $l_p$ in Figure 2. The abscissa of the intercept between the horizontal dashed line representing $<r_{EE}{}^2> = (N_{blob}{}^\infty \times b)^2$ and the line corresponding to the right-hand side of the KPE yields $l_p$ for the PyEG$_5$-PEG$_n$MA series under consideration.

$$< r_{EE}^2 >_{blob} = (N_{blob}^\infty \times b)^2 = 2l_p(b \times < N_{blob} >) - 2l_p^2 \left[ 1 - \exp\left( -\frac{b \times < N_{blob} >}{l_p} \right) \right] \tag{3}$$

## 3. Results and Discussion

A series of pyrene-labeled poly(oligo(ethylene glycol) methyl ether methacrylate)s (PyEG$_5$-PEG$_n$MA with $n$ = 0, 3, 4, 5, 7, 9, and 19) were synthesized using a grafting through technique by mainly free radical copolymerization of the same penta(ethylene glycol) 1-pyrenemethyl ether methacrylate (PyEG$_5$MA) and different oligo(ethylene glycol) methyl ether methacrylate (EG$_n$MA) macromonomers. Their chemical structure, the number ($N_S$) of atoms in each side chain, and the molecular weight of the structural unit ($MW$(SU)) were presented in Table 1. The number average molecular weight ($M_n$) and dispersity (Đ) of all PyEG$_5$-PEG$_n$MA samples were determined by gel permeation chromatography and are listed in Table 2. Variations in $M_n$ and Đ were observed from sample-to-sample in Table 2 due to the relative purity and reactivity of the different monomers. Nevertheless, the $M_n$ values were sufficiently large to ensure that all polymer samples were constituted of many *blobs*, which enabled the analysis of the fluorescence decays with the FBM, that could handle these samples, whose Đ values greater than 1.0 indicate that they are polydisperse. The design of the PyEG$_5$-PEG$_n$MA constructs was carefully considered. It was established in an earlier study with pyrene-labeled poly($n$-butyl methacrylate)s, that the motion of the pyrenyl group became uncorrelated from the motion of the main chain, when a 1-pyrenemethoxy derivative was connected to the main polymethacrylate backbone by a linker made of two or more ethylene glycol units [27]. The use of a penta(ethylene glycol) linker for the PyEG$_5$-PEG$_n$MA samples thus ensured that an excited pyrenyl label would probe a well-defined sub-volume ($V_{blob}$) of the PBBs, referred to as a *blob* within the FBM framework, that would be unaffected by any main chain motion. In turn, this condition implied that each PBB was being probed over the same length scale defined by the same $V_{blob}$ for all PyEG$_5$-PEG$_n$MA constructs considered in this study.

The SSF spectra for all pyrene contents of each PyEG$_5$-PEG$_n$MA series were acquired in acetonitrile, tetrahydrofuran (THF), *N*,*N*-dimethylformamide (DMF), and dimethyl sulfoxide (DMSO) and are presented in Figures S6–S9 in the SI. The spectra for all pyrene contents of the PyEG$_5$-PEG$_4$MA series in each solvent are shown in Figure 3.
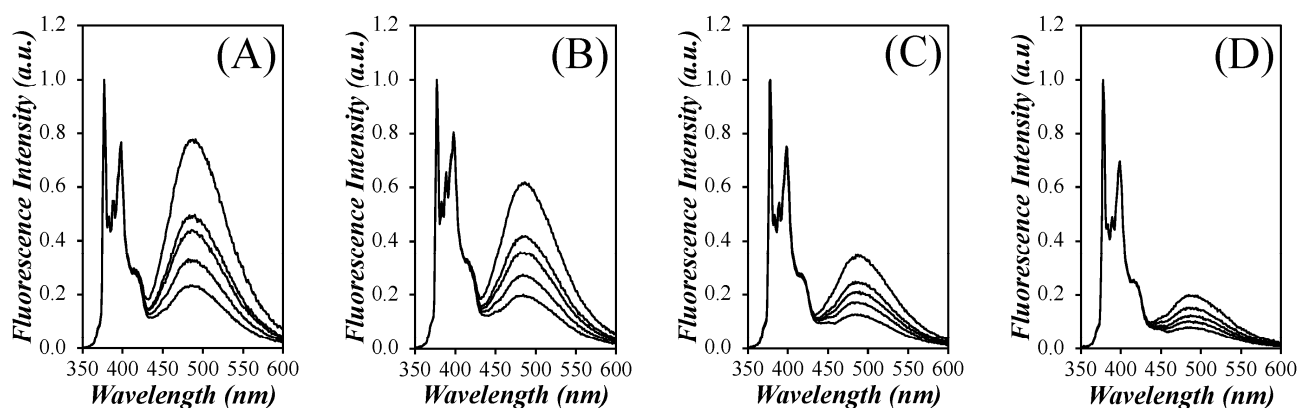


**Figure 3.** Steady-state fluorescence spectra of the PyEG$_5$-PEG$_4$MA samples in (**A**) acetonitrile, (**B**) THF, (**C**) DMF, and (**D**) DMSO with pyrene contents ranging from 1.2 to 3.1 mol % shown from bottom to top. [$Py$] = $2.5 \times 10^{-6}$ M; $\lambda_{ex}$ = 344 nm.

The spectra were normalized to the first peak of the monomer emission, $I_1$, which is the 0-0 transition of pyrene. They showed the characteristic fluorescence peaks between 375 and

410 nm for the pyrene monomer with the broad and structureless excimer emission centered at 480 nm. It is apparent from Figure 3, that more excimer is produced in acetonitrile than in THF, DMF, and DMSO, with DMSO producing the least amount of excimer. The $I_E/I_M$ ratio was calculated to quantify the efficiency of pyrene excimer formation (PEF) for the different constructs in different solvents. The $I_E/I_M$ ratio is proportional to the local concentration of pyrene, $[Py]_{loc}$, and the rate constant for PEF through diffusive encounters, $k_{diff}$, as indicated by Equation (4).

$$\frac{I_E}{I_M} \sim k_{diff} \times [Py]_{loc} \tag{4}$$

The $I_E/I_M$ ratios were plotted as a function of pyrene content for each PyEG$_5$-PEG$_n$MA sample in Figure S10. They yielded straight lines over a wide range of pyrene contents and the slope of these lines ($m(I_E/I_M)$) was plotted as a function of $MW(SU)$ in Figure 4. In each solvent, the slope $m(I_E/I_M)$ decreased as $MW(SU)$ increased for the PyEG$_5$-PEG$_n$MA samples with $n$ equal to 0, 3, 4, and 5, respectively. This decrease was attributed to an extension of the polymer backbone, that resulted from increased crowding of the volume surrounding the main chain with increasing $MW(SU)$. Main chain extension reduced the number of encounters between the pyrenyl terminals of the PyEG$_5$ side chains, which was associated with a decrease in $[Py]_{loc}$ in Equation (3). The decrease in $m(I_E/I_M)$ continued until an $MW(SU)$ of 408 g/mol for PyEG$_5$-PEG$_7$MA was reached, after which $m(I_E/I_M)$ seemed to plateau for $MW(SU)$ values of 500 and 950 g/mol for PyEG$_5$-PEG$_9$MA and PyEG$_5$-PEG$_{19}$MA, respectively. The plateau region observed for $N_S$ values larger than 400 g/mol indicated that a further increase in side chain length would not result in an increase in main chain extension, probably because the main chain was, or was close to being, fully extended on the length scale probed by an excited pyrene. The $m(I_E/I_M)$-*vs.*-$MW(SU)$ trends shown in Figure 4 suggested that the steric hindrance generated by the side chains influence a region inside the polymeric bottlebrush (PBB) volume, that is close to the main chain and where the shorter EG$_n$ side chains have the strongest effect. As the side chains become long enough to expand past the local region close to the main chain and into the mostly empty space away from the main chain, their effect on the main chain becomes less important, resulting in the plateau observed for large side chain lengths in the $m(I_E/I_M)$-*vs*-$MW(SU)$ plot in Figure 4. Similar saturation effects with increasing side chain length have already been reported for PBBs [20,28].

The $m(I_E/I_M)$ slopes in Figure 4 were also found to be larger in acetonitrile, followed by THF, DMF, and DMSO. This trend reflects the influence of the solvent viscosity, $\eta$. The viscosity of acetonitrile, THF, DMF, and DMSO at 25 °C equals 0.37, 0.46, 0.79, and 1.99 mPa·s, respectively [29]. Since $k_{diff}$ is inversely proportional to solvent viscosity [30], acetonitrile with the lowest $\eta$ yielded the largest $k_{diff}$ values in Equation (4) and the largest $m(I_E/I_M)$ slopes in Figure 4A. Similarly, DMSO being the most viscous solvent yielded the lowest $m(I_E/I_M)$ slopes in Figure 4D. THF and DMF with their intermediate $\eta$ values resulted in intermediate $m(I_E/I_M)$ slopes. As was pointed out in earlier reports [31,32], solvent viscosity, while important, is not the only parameter affecting $k_{diff}$. The probability $p$, of forming an excimer upon an encounter between an excited and a ground-state pyrenyl label, depends also on the solvent, and its value can offset the relationship expected between $k_{diff}$ and $\eta^{-1}$ [30]. Consequently, the interpretation of the parameter $m(I_E/I_M)$ obtained from the analysis of the steady-state fluorescence spectra offers only a qualitative description of the fluorescence results.

A more quantitative measure of polymer stiffness, such as the persistence length ($l_p$), can only be retrieved from PEF measurements through the global analysis of the monomer and excimer decays acquired with the PyEG$_5$-PEG$_n$MA samples as was performed earlier with the PyBut-PEG$_n$MA samples [20]. The determination of $N_{blob}$ for the PyEG$_5$-PEG$_n$MA samples represents the second step in the procedure applied to obtain $l_p$ as described in Figure 1. The FBM analysis of the decays yields the number $N_{blob}$ of methacrylate units that can pack inside a *blob*, which is the volume probed by an excited pyrenyl label. Lower $N_{blob}$ values are obtained for stiffer chains, that bend less efficiently. The fluorescence decays

were acquired in acetonitrile, THF, DMF, and DMSO and the FBM yielded $N_{blob}$, which was plotted as a function of pyrene content in Figure 5A–D.
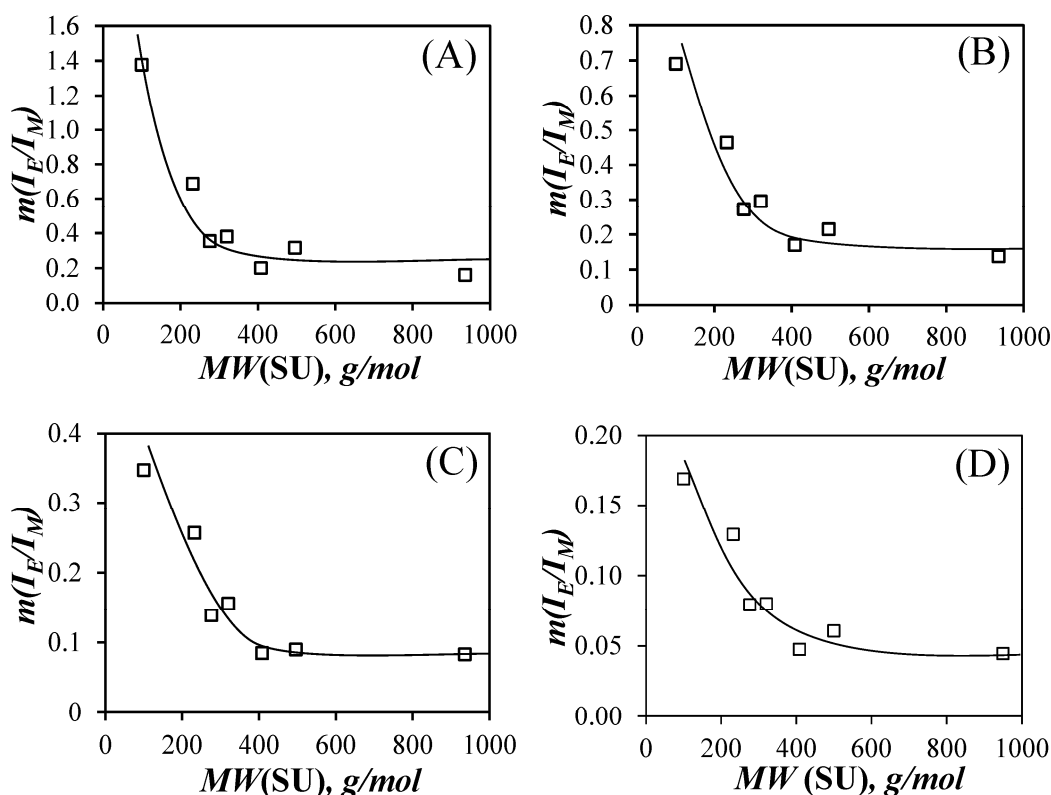


**Figure 4.** Plot of $m(I_E/I_M)$ versus $MW$(SU) for the PyEG$_5$-PEG$_n$MA PBBs in (**A**) acetonitrile, (**B**) THF, (**C**) DMF, and (**D**) DMSO.

　　　Within experimental error, $N_{blob}$ remained constant with pyrene content in Figure 5A–D. $N_{blob}$ was averaged over all pyrene contents for all the samples of the same PyEG$_5$-PEG$_n$MA series in the same solvent to yield $<N_{blob}>$, which was plotted as a function of the molecular weight of a structural unit ($MW$(SU)) in Figure 5E–H. The plots shown in Figure 5E–H display some interesting features. For each solvent, $<N_{blob}>$ was found to decrease with increasing side chain length reflecting the increased extension of the PEG$_n$MA backbone with increasing side chain length. $<N_{blob}>$ reached a plateau value ($N_{blob}^\infty$) for the largest side chains indicating that the polymethacrylate backbone appeared fully extended over the length scale probed by an excited pyrenyl label. Finally, $<N_{blob}>$ for the PyEG$_5$-PEG$_n$MA samples with an 18-atom-long linker connecting pyrene to the polymethacrylate backbone was significantly larger than $<N_{blob}>$ obtained earlier for the PyBut-PEG$_n$MA samples with a 6-atom-long spacer between pyrene and the polymethacrylate backbone as indicated by the difference between the dashed and solid lines in Figure 5E–H. These differences in $<N_{blob}>$ between the PyBut-PEG$_n$MA and PyEG$_5$-PEG$_n$MA samples reflect the longer reach of the pyrene derivative used for the latter series.

　　　Another interesting feature in the plots shown in Figure 5E–H was that for the same pyrene content, $<N_{blob}>$ decreased with increasing solvent viscosity. While this effect had also been observed for the PyBut-PEG$_n$MA samples [20], it was much more pronounced for the PyEG$_5$-PEG$_n$MA samples. This effect could be better visualized in Figure 6A, where $<N_{blob}>$ was plotted as a function of $N_S^{-2}$, with $N_S$ being the number of non-hydrogen atoms in the PEG$_n$MA side chains equal to $3 + 3 \times n$ for a given PEG$_n$MA sample. The $<N_{blob}>$-$vs$-$N_S^{-2}$ plots in Figure 6A yielded straight lines, except for the $<N_{blob}>$ value of PyEG$_5$-PEG$_0$MA, which departed from the linear behavior in all solvents. The largest $<N_{blob}>$ values were found in acetonitrile, followed by THF, DMF, and DMSO, where the lowest $<N_{blob}>$ values were obtained.

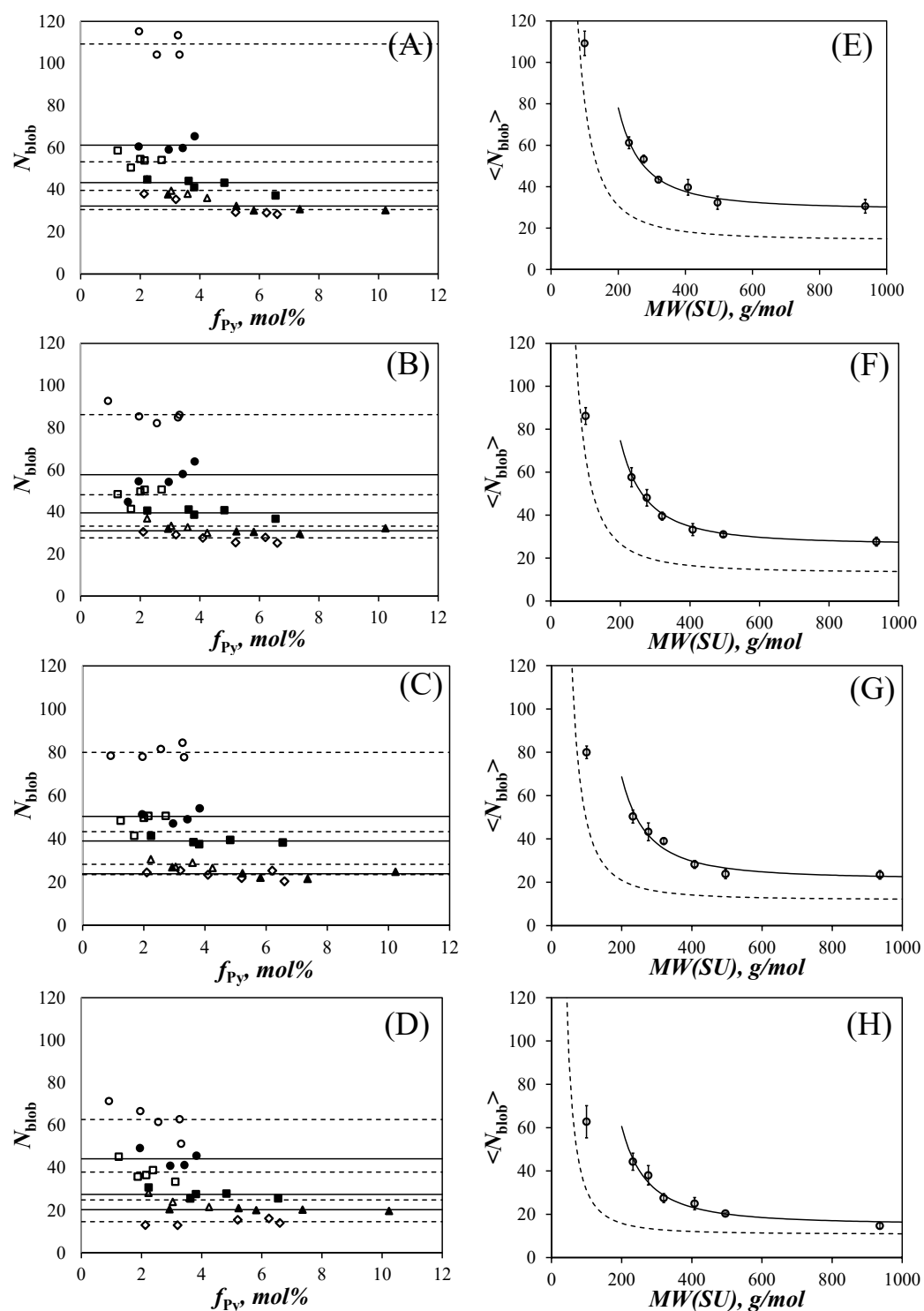**Figure 5.** Plots of (**A–D**) $N_{blob}$ as a function of pyrene content for (⬭) PyEG$_5$-PEG$_0$MA, (●) PyEG$_5$-PEG$_3$MA, (▢) PyEG$_5$-PEG$_4$MA, (■) PyEG$_5$-PEG$_5$MA, (△) PyEG$_5$-PEG$_7$MA, (▲) PyEG$_5$-PEG$_9$MA, and (◆) PyEG$_5$-PEG$_{19}$MA and (**E–H**) $<N_{blob}>$ as a function of $MW$(SU) in (**A,E**) acetonitrile, (**B,F**) THF, (**C,G**) DMF, and (**D,H**) DMSO. Lines: prediction for the $<N_{blob}>$ values for (solid) the PyEG$_5$-PEG$_n$MA samples with Equation (8) and (dashed) the PyBut-PEG$_n$MA samples.
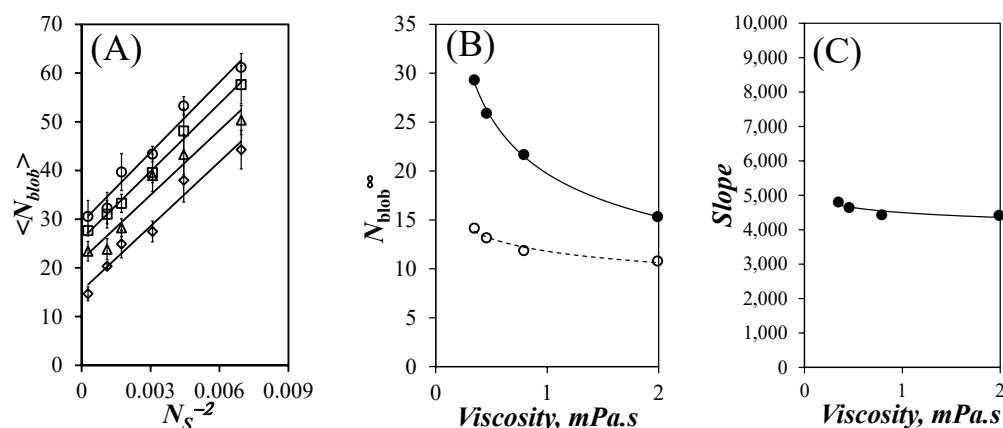
**Figure 6.** (**A**) Plot of $<N_{blob}>$ as a function of $N_S^{-2}$ for the PyEG$_5$-PEG$_n$MA samples except for $n = 0$ in (○) acetonitrile, (▪) THF, (▲) DMF, and (◆) DMSO. (**B**) Plot of $N_{blob}^\infty$ as a function of solvent viscosity for the (●) PyEG$_5$-PEG$_n$MA and (○) PyBut-PEG$_n$MA samples. (**C**) Plot of the slopes of the straight lines in Figure 6A as a function of solvent viscosity.

The value of $<N_{blob}>$ for poly(methyl methacrylate) in all solvents was lower than that expected from the straight lines shown in Figure 6A. This is probably because for infinite $N_S^{-2}$, the polymethacrylate backbone still retains some residual stiffness preventing it from collapsing and packing an infinite number of methacrylate monomers when $N_S$ is infinitely small. Consequently, a limit must be reached experimentally, that prevents $<N_{blob}>$ from taking an infinite value for infinitely small side chains, as would be otherwise predicted from the straight lines shown in Figure 6A. It is thus reasonable that the $<N_{blob}>$ values obtained for the PyEG$_5$-PEG$_n$MA samples having shorter side chains, such as for poly(methyl methacrylate), did not obey the linear $<N_{blob}>$-vs-$N_S^{-2}$ found for the PyEG$_5$-PEG$_n$MA samples with longer side chains in Figure 6A. Extrapolating the straight lines in Figure 6A to the Y-intercept yielded $N_{blob}^\infty$ representing the number of methacrylate units encompassed inside a *blob* for a fully extended polymethacrylate backbone. $N_{blob}^\infty$ was plotted as a function of solvent viscosity in Figure 6B for the PyEG$_5$-PEG$_n$MA samples along with the $N_{blob}^\infty$ values found earlier for the PyBut-PEG$_n$MA samples. The determination of $N_{blob}^\infty$ represents the third step in the methodology developed to determine $l_p$ as shown in Figure 1.

$N_{blob}^\infty$ for the PyEG$_5$-PEG$_n$MA samples was much larger than for the PyBut-PEG$_n$MA samples [20] reflecting the longer reach of the linker for the PyEG$_5$ derivative [27]. The difference between the $N_{blob}^\infty$ values obtained for the PyBut-PEG$_n$MA and PyEG$_5$-PEG$_n$MA samples decreased with increasing viscosity since a larger solvent viscosity hinders the deployment of the pyrenyl labels at the end of the long EG$_5$ linker in the PyEG$_5$-PEG$_n$MA samples during the finite time that the pyrenyl label remains excited. This effect is much less pronounced for the PyBut-PEG$_n$MA samples for which the much shorter butyl linker enables the full deployment of the pyrenyl label while it remains excited. Indeed, the $N_{blob}^\infty$ dependency on solvent viscosity for the PyBut-PEG$_n$MA samples in Figure 6B is much weaker than that for the PyEG$_5$-PEG$_n$MA samples.

The slopes of the straight lines obtained in Figure 6A were plotted as a function of solvent viscosity in Figure 6C. The slopes showed little dependency on solvent viscosity. The $N_{blob}^\infty$ values and the slopes for the PyEG$_5$-PEG$_n$MA samples could be fitted with power laws, whose empirical expressions are given as Equations (5) and (6), respectively. In turn, the equations for $N_{blob}^\infty$ and the slopes could be rearranged to yield the bending function ($f_b(\eta, MW(SU))$) in Equation (7). Multiplying $N_{blob}^\infty$ by the bending function yielded $<N_{blob}>$ in Equation (8), which was found to properly describe the experimental $<N_{blob}>$ values in Figure 5E–H for $MW(SU)$ greater than 200 g/mol.

$$N_{blob}^\infty = 19.732 \times \eta^{-0.365} \tag{5}$$

$$slope = 4498.3 \times \eta^{-0.046} \tag{6}$$

$$f_b(\eta, MW(SU)) = 1.0 + \frac{227.9698 \times \eta^{0.319}}{(3 + 3 \times (MW(SU) - 100)/44)^2} \tag{7}$$

$$< N_{blob} > = N_{blob}^\infty \times f_b(\eta, MW(SU)) \tag{8}$$

The parametrization of the $<N_{\text{blob}}>$ values with Equation (8) could now be applied to predict the persistence length ($l_\text{p}$) for any hypothetical molar mass $MW(SU)$ greater than 200 g/mol of a $PyEG_5$-$PEG_n MA$ sample in any solvent as depicted in Figure 2. This was achieved by solving for $l_\text{p}$ in Equation (3) representing the Kratky–Porod equation [24] modified to represent the polymer segment made of $<N_{\text{blob}}>$ structural units of contour length $<N_{\text{blob}}> \times b$, where $b$ is the length of a methacrylate monomer typically taken to equal 0.25 nm [25,26], inside a *blob* with an end-to-end distance $<r_{\text{EE}}^2>_{\text{blob}}$ [20]. In turn, since all $PyEG_5$-$PEG_n MA$ constructs use the same pyrene derivative, the excited pyrenyl label probes the same volume for all the samples, including those fully extended $PyEG_5$-$PEG_n MA$ samples with infinitely long side chains for which $<r_{\text{EE}}^2>_{\text{blob}}$ is simply equal to $N_{\text{blob}}^\infty \times b$, where the expression of $N_{\text{blob}}^\infty$ was given in Equation (5).

Since the left-hand side of Equation (3) is known, Equation (3) could be solved to retrieve $l_\text{p}$ for any $<N_{\text{blob}}>$ value obtained with Equation (8) for any solvent viscosity and $MW(SU)$ greater than 200 g/mol. The resulting $l_\text{p}$-*vs*-$N_\text{S}^2$ plots are shown in Figure 6. $l_\text{p}$ increased linearly with increasing $N_\text{S}^2$ in all solvents considered. The linear increase in $l_\text{p}$ with $N_\text{S}^2$ agrees with theoretical predictions [33]. The predicted trends obtained with $l_\text{p}$ for the $PyEG_5$-$PEG_n MA$ samples showed a much closer agreement with the experimental data points compared to the trends obtained with $l_\text{p}$ for the $PyBut$-$PEG_n MA$ samples, probably because the longer linker of the $PyEG_5$ derivative resulted in larger $<N_{\text{blob}}>$ values which were retrieved with better accuracy.

As for the $l_\text{p}$ values obtained with the $PyBut$-$PEG_n MA$ samples [20], solvent viscosity affected the $l_\text{p}$ values retrieved for the $PyEG_5$-$PEG_n MA$ samples. However, the effect of solvent viscosity on $l_\text{p}$ was opposite between the two polymer series. Whereas an increase in solvent viscosity led to an increase in $l_\text{p}$ for the $PyBut$-$PEG_n MA$ samples, it was accompanied by a decrease in $l_\text{p}$ for the $PyEG_5$-$PEG_n MA$ samples. The reason for the opposite trends resided in the different spacers connecting pyrene to the polymethacrylate backbone. In the case of the $PyBut$-$PEG_n MA$ samples, the volume of a *blob* ($V_{\text{blob}}$) was little affected by solvent viscosity [20], as indicated by the small changes in $N_{\text{blob}}^\infty$ with solvent viscosity observed in Figure 6B. The small dependency of $N_{\text{blob}}^\infty$ on solvent viscosity enabled the short 6-atom-long spacer to fully deploy, allowing the pyrenyl label to probe a constant $V_{\text{blob}}$ regardless of solvent viscosity. An increase in solvent viscosity for the $PyBut$-$PEG_n MA$ series resulted in weaker PEF, which was erroneously attributed to a stiffening of the chain, resulting in an increase in $l_\text{p}$ based on the Kratky–Porod equation. In contrast, $V_{\text{blob}}$ was much more strongly affected by solvent viscosity for the longer 18-atom-long penta(ethylene glycol) spacer of the $PyEG_5$-$PEG_n MA$ sample, as illustrated by the significant decrease in $N_{\text{blob}}^\infty$ in Figure 6B. The inability of the $PyEG_5$ derivative to fully deploy while a pyrenyl label remained excited meant that the excited pyrene probed a smaller $V_{\text{blob}}$ with increasing solvent viscosity. Since the density of a *blob* with a polymer segment of size $N_{\text{blob}}$ increases with decreasing $N_{\text{blob}}$ as $N_{\text{blob}}/N_{\text{blob}}^{3/2} = N_{\text{blob}}^{-0.5}$ [15], a smaller *blob* appeared denser, yielding a smaller $l_\text{p}$ for the $PyEG_5$-$PEG_n MA$ samples as observed in Figure 7A–D.
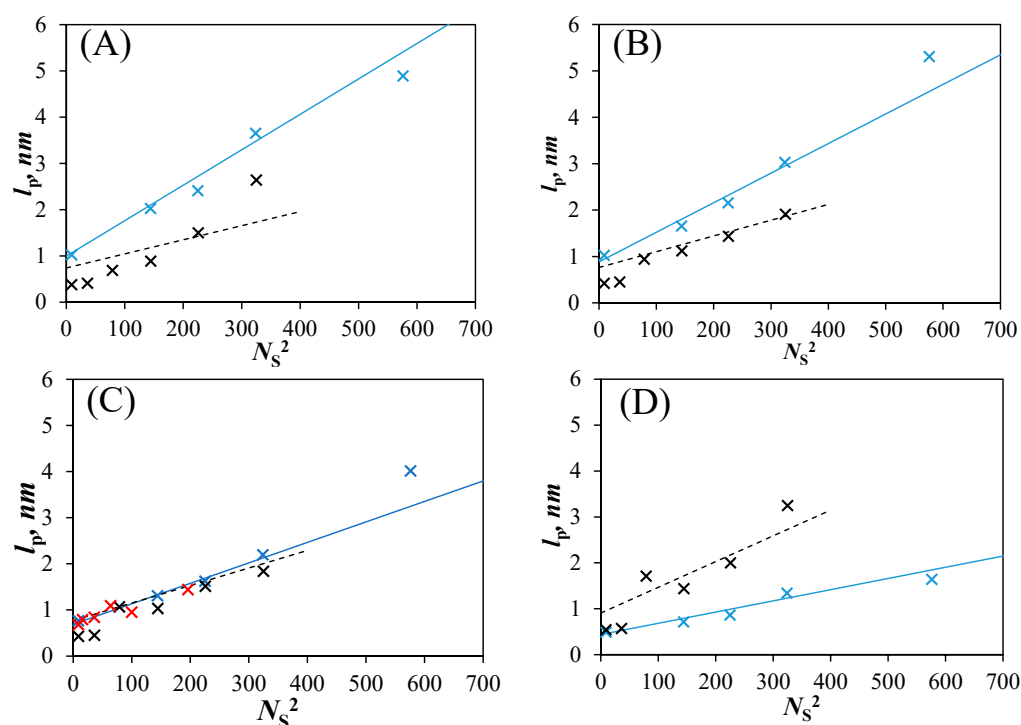
**Figure 7.** Plot of $l_p$ as a function of $N_S^2$ for the ($\times$) PyEG$_5$-PEG$_n$MA and ($\times$) PyBut-PEG$_n$MA samples in (**A**) acetonitrile for PyPEG$_5$-PEG$_n$MA and acetone for PyBut-PEG$_n$MA, (**B**) THF, (**C**) DMF, and (**D**) DMSO. ($\times$) $l_p$ values obtained for a series of poly(alkyl methacrylate) [11]. Lines: (solid blue) predicted $l_p$ values for the PyPEG$_5$-PEG$_n$MA samples based on Equations (3)–(8) and (dashed black) predicted values for the PyBut-PEG$_n$MA samples [20].

Since effects induced by solvent viscosity on $<N_{blob}>$ were eliminated when working in a solvent with a viscosity of 0.74 mPa.s approaching that of 0.79 mPa.s for DMF according to molecular mechanics optimizations (MMO) [20], the $l_p$ values obtained in DMF were expected to best represent the persistence length of PEG$_n$MA. As it turned out, the $l_p$ values retrieved for the PyBut-PEG$_n$MA and PyEG$_5$-PEG$_n$MA samples showed excellent agreement in DMF in Figure 7C. Furthermore, the $l_p$ values retrieved in DMF matched very closely those reported for a series of poly(alkyl methacrylate)s of similar $MW$(SU) [11], where the poly(alkyl methacrylate)s have been shown to behave similarly to PEG$_n$MA over the short length scales probed by an excited pyrenyl label [20]. The concurring trends presented in Figure 7C for the $l_p$ values retrieved for several polymethacrylates by different procedures provide solid validation of the PEF-based method for measuring the persistence length of these polydisperse polymethacrylate samples.

Another interesting observation in Figure 7C was that the straight lines representing the $l_p$-$vs$-$N_S^2$ trends in Figure 7C did not pass through the origin for an infinitely short side chain. The non-zero Y-intercept is a result of the intrinsic stiffness of the polymethacrylate backbone, which prevents $l_p$ from reaching zero for an infinitely short side chain. In turn, this conclusion implies that $<N_{blob}>$ cannot take infinite values for infinitely short side chains as expected from the $<N_{blob}>$-$vs$-$N_S^{-2}$ straight lines shown in Figure 6A. Instead, $<N_{blob}>$ should reach a constant value for shorter side chains approaching the $<N_{blob}>$ value expected for the unsubstituted polymethacrylate backbone. This most certainly explains why the $<N_{blob}>$ value for the PyPEG$_5$-PEG$_0$MA series did not fall on the straight lines in Figure 6A.

In order to properly predict the $<N_{blob}>$ values that should be obtained for polymethacrylates having short side chains, Equations (9) and (10) were used to parametrize the intercepts and slopes of the $l_p$-$vs$-$N_S^2$ straight lines in Figure 6A–D. Combining Equations (9) and (10) yielded the persistence length for any $MW$(SU) and solvent viscosity, which could then be

employed with Equation (3) to extract $<N_{\text{blob}}>$. The resulting plots of $<N_{\text{blob}}>$ as a function of $MW$(SU) are shown in Figure 8A–D for acetonitrile, THF, DMF, and DMSO.
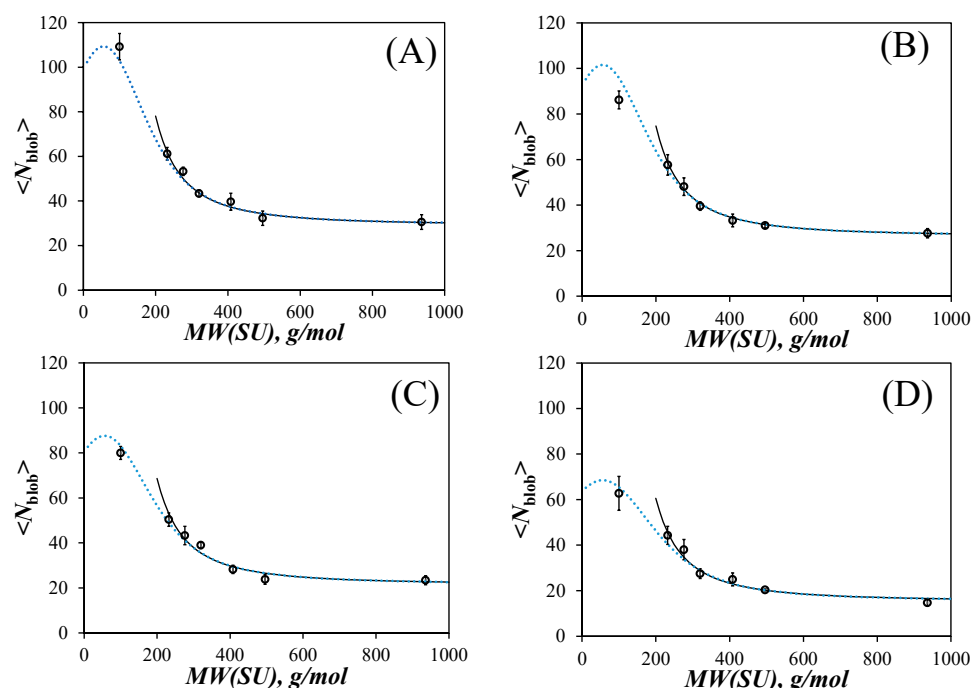


**Figure 8.** Plots of $<N_{\text{blob}}>$ as a function of $MW$(SU) for the $PyEG_5$-$PEG_n MA$ samples in (**A**) acetonitrile, (**B**) THF, (**C**) DMF, and (**D**) DMSO. Lines: $l_p$ calculated according to (solid black) Equation (8) and (dotted blue) back calculated from Equation (3).

The new trends pass through most of the data points including the $<N_{\text{blob}}>$ value for $PyEG_5$-$PEG_0 MA$. Instead of $<N_{\text{blob}}>$ tending to infinity for infinitely small side chains, $<N_{\text{blob}}>$ goes through an inflection point as it approaches $MW$(SU) = 100 g/mol for poly(methyl methacrylate) before passing through a maximum and intercepting the $Y$-axis at a finite, non-zero value. The small dip observed for short side chains before the maximum in the plots of Figure 8 is certainly an artefact resulting from the mathematical handling of the Kratky–Porod equation with the linear relationship between $l_p$ and $N_S{}^2$ in Figure 7 to predict $<N_{\text{blob}}>$. Despite this mathematical artefact, the plots of $<N_{\text{blob}}>$-*vs*-$MW$(SU) in Figure 8 provide a physically more realistic depiction of the behavior of $<N_{\text{blob}}>$ expected as the side chains become infinitely short, because $<N_{\text{blob}}>$ no longer diverges to infinity as would be otherwise predicted with Equation (8).

$$l_p(\text{intercept}) = 0.610 \times \eta^{-0.469} \tag{9}$$

$$l_p(\text{slope}) = 3.82 \times 10^{-3} \times \eta^{-0.654} \tag{10}$$

The backbone conformation of $PEG_{19}MA$ was further investigated by atomic force microscopy (AFM) to visualize individual $PEG_{19}MA$ macromolecules, which were prepared without pyrene. This sample had a number ($M_n$) and weight ($M_w$) average molecular weight of 134,000 and 193,000 g·mol$^{-1}$, respectively. Individual polymer molecules were observed in Figure 9 ranging in length from 20 to 90 nm, in diameter from 10 to 20 nm, and in height from 0.5 to 1 nm. These results are consistent with the expected dimensions of these macromolecules considering that a fully extended $PEG_{19}MA$ macromolecule would have a number average contour length of ~35 nm and an average width of ~16 nm.
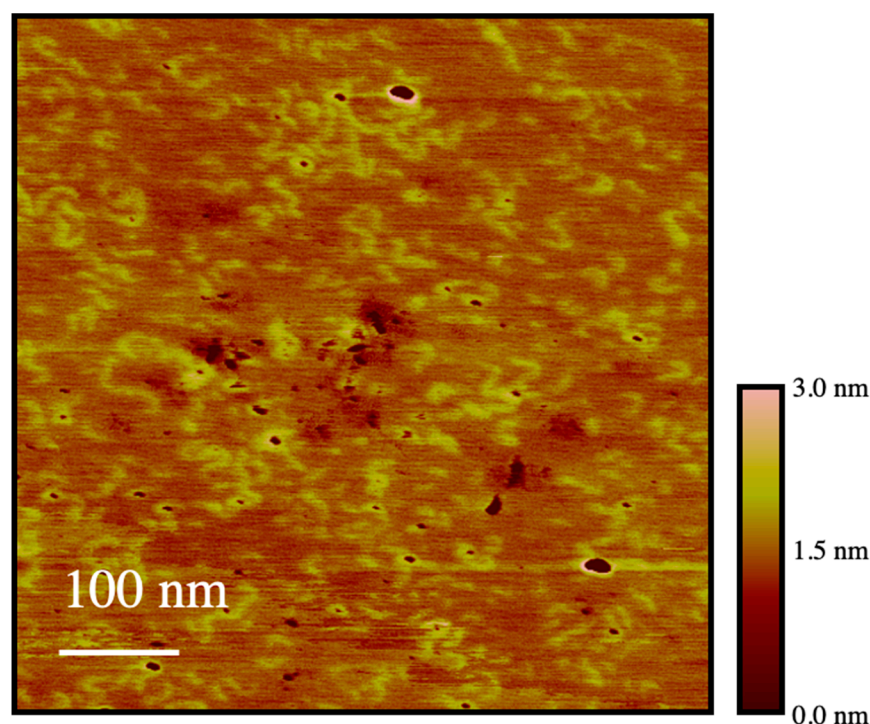
**Figure 9.** AFM topography image of $PEG_{19}MA$ spin-coated on a freshly cleaved mica surface from a 10 mg/L solution in THF.

Furthermore, the AFM image shown in Figure 9 clearly demonstrates the presence of isolated macromolecules with no indication of aggregation. This observation eliminates the possibility that $PEG_{19}MA$ could aggregate, as has been found for PBBs prepared with longer poly(ethylene oxide) side chains, which have been shown to crystalize resulting in the formation of crystalsomes [34]. Figure 9 demonstrates that this is not the case for $PEG_{19}MA$. Although the chains observed in Figure 9 show some curvature, the steric hindrance generated by their side chains prevents them from adopting a fully coiled conformation.

The image shown in Figure 9 complements the conclusions drawn from the plateau reached for $m(I_E/I_M)$ in Figure 4 and for $N_{blob}$ in Figure 5E–H obtained by steady-state and time-resolved fluorescence, respectively. These plateaus were defined mostly by the $m(I_E/I_M)$ and $N_{blob}$ values obtained with samples from the $PyEG_5$-$PEG_{19}MA$ series, and they were rationalized by evoking the stiffening and extension of the polymer backbone. Such a stiffening is clearly visible in the AFM picture where the $PEG_{19}MA$ macromolecules appear as WLCs.

**4. Conclusions**

The PEF-based method introduced earlier to determine the persistence length of polymers [20] that are polydisperse was improved by widening the volume probed by an excited pyrenyl label. This was achieved by using a penta(ethylene glycol) 1-pyrenemethyl ether derivative to generate an 18-atom-long spacer between the pyrenyl label and the polymethacrylate backbone instead of the sort 6-atom-long spacer obtained with the commercially available 1-pyrenebutanol derivative [20]. Considering that $N_{blob}^{\infty}$ ranged from 15 in DMSO to 29 in acetonitrile for the $PyEG_5$-$PEG_nMA$ samples, an excited pyrenyl label could probe a *blob*, whose diameter equal to $N_{blob}^{\infty} \times b$ ranged between 3.8 nm in DMSO and 7.3 nm in acetonitrile, significantly larger than the *blobs* with a 3.0 nm diameter obtained with the $PyBut$-$PEG_nMA$ samples [20]. The larger *blobs* probed with the $PyEG_5$-$PEG_nMA$ samples enabled larger persistence lengths to be measured, reaching up to 4.0 nm compared to the maximum persistence length of 2.0 nm reached earlier with the $PyBut$-$PEG_nMA$ samples. Excellent agreement was obtained for the persistence lengths determined with the

PyBut-PEG$_n$MA and PyEG$_5$-PEG$_n$MA samples in DMF, a solvent whose viscosity happens to eliminate the effects induced on $<N_{blob}>$ by solvent viscosity. By spreading $<N_{blob}>$ over a much wider range of $MW$(SU) values in Figure 5E–H, three regimes could be clearly identified for different lengths of side chains in Figure 8. On the one hand, short side chains yield $<N_{blob}>$ values that change little with side chain length as $<N_{blob}>$ reflects the intrinsic flexibility of the unsubstituted polymethacrylate backbone. On the other hand, very long side chains induce a fully extended conformation of the PEG$_n$MA backbone resulting in $<N_{blob}>$ taking a constant value with side chain length equal to $N_{blob}^\infty$. Significant changes in $<N_{blob}>$ are only observed for PEG$_n$MA samples with intermediate side chain lengths between two and nine ethylene glycol units. In turn, the range of $<N_{blob}>$ values is directly related to the range of persistence lengths that can be retrieved from PEF measurements conducted with PEG$_n$MA samples labeled with a given pyrene derivative, as shown with the plots in Figure 8. Consequently, this study confirms the potential of PEF-based methods to characterize the persistence length of polydisperse polymers in any organic solvent, which should enable the determination of the unknown persistence length of many polymers.

**Supplementary Materials:** The following supporting information can be downloaded at: https://www.mdpi.com/article/10.3390/polym15193958/s1, Equations used in the FBM analysis, Figure S1. $^1$H NMR spectrum of penta(ethylene glycol) mono *p*-toluene sulfonate, Figure S2. $^1$H NMR spectrum of 1-pyrenemethyl ether penta(ethylene glycol), Figure S3. $^1$H NMR spectrum of penta(ethylene glycol) methyl ether methacrylate, Figure S4. $^1$H NMR spectrum of PyEG$_5$(3.6)-PEG$_5$MA, Figure S5. GPC traces in THF with DRI and absorption detector for the representative PyEG$_5$-PEG$_n$MA samples, Figure S6. SSF spectra of PyEG$_5$-PEG$_n$MA samples in acetonitrile, Figure S7. SSF spectra of PyEG$_5$-PEG$_n$MA samples in THF, Figure S8. SSF spectra of PyEG$_5$-PEG$_n$MA samples in DMF, Figure S9. SSF spectra of PyEG$_5$-PEG$_n$MA samples in DMSO, Figure S10. Plot of $I_E/I_M$ ratio versus pyrene content for PyEG$_5$-PEG$_n$MA in acetonitrile, THF, DMF, and DSMO, Figure S11. Global FBM analysis of the monomer and excimer fluorescence decays for the PyEG$_5$(2.6)-PEG$_0$MA, Tables S1–S12. Parameters retrieved from the FBM analysis of the monomer and excimer decays for the PyEG$_5$-PEG$_n$MA samples in acetonitrile, THF, DMF, and DMSO.

**Author Contributions:** J.L.T. conducted all the experimental work except the microscopy experiment and wrote the first draft of the manuscript; H.L. applied his earlier finding that DMF is the solvent where viscosity effects cancel out to demonstrate that the persistence lengths obtained with the PyBut-PEG$_n$MA, PyEG$_5$-PEG$_n$MA, and poly(alkyl methacrylate) matched in this solvent; J.D. proposed the project, funded the research, provided supervision and guidance for the mathematical derivations, and wrote the final version of the manuscript; L.Z. acquired the AFM images and interpreted them; K.T.L. supervised the AFM work and reviewed the manuscript. All authors have read and agreed to the published version of the manuscript.

**Data Availability Statement:** Data will be made available upon request.

## References

1. Sherck, N.; Webber, T.; Brown, D.R.; Keller, T.; Barry, M.; DeStefano, A.; Jiao, S.; Segalman, R.A.; Fredrickson, G.H.; Shell, M.S.; et al. End-to-End Distance Probability Distributions of Dilute Poly(ethylene oxide) in Aqueous Solution. *J. Am. Chem. Soc.* **2020**, *142*, 19631–19641. [CrossRef] [PubMed]
2. Tsuji, T.; Norisuye, T.; Fujita, H. Dilute Solution of Bisphenol A Polycarbonate. *Polym. J.* **1975**, *7*, 558–569. [CrossRef]
3. Odijk, T. On the statistics and dynamics of confined or entangled stiff polymers. *Macromolecules* **1983**, *16*, 1340–1344. [CrossRef]
4. Morse, D.C. Viscoelasticity of Concentrated Isotropic Solutions of Semiflexible Polymers. 1. Model and Stress Tensor. *Macromolecules* **1998**, *31*, 7030–7043. [CrossRef]
5. Morse, D.C. Viscoelasticity of Concentrated Isotropic Solutions of Semiflexible Polymers. 2. Linear Response. *Macromolecules* **1998**, *31*, 7044–7067. [CrossRef]
6. Schuldt, C.; Schnauß, J.; Händler, T.; Glaser, M.; Lorenz, J.; Golde, T.; Käs, J.A.; Smith, D.M. Tuning Synthetic Semiflexible Networks by Bending Stiffness. *Phys. Rev. Lett.* **2016**, *117*, 197801. [CrossRef]

7.  Tassieri, M. Dynamics of Semiflexible Polymer Solutions in the Tighty Entangled Concentration Regime. *Macromolecules* **2017**, *50*, 5611–5618. [CrossRef]

8.  Nikoubashman, A. Ordering, phase behavior, and correlations of semiflexible polymers in confinement. *J. Chem. Phys.* **2021**, *154*, 090901. [CrossRef]

9.  Kikuchi, M.; Nakano, R.; Jinbo, Y.; Saito, Y.; Ohno, S.; Togashi, D.; Enomoto, K.; Narumi, A.; Haba, O.; Kawaguchi, S. Graft Density Dependence of Main Chain Stiffness in Molecular Rod Brushes. *Macromolecules* **2015**, *48*, 5878–5886. [CrossRef]

10. Zhang, B.; Gröhn, F.; Pedersen, J.S.; Fischer, K.; Schmidt, M. Conformation of Cylindrical Brushes in Solution: Effect of Side Chain Length. *Macromolecules* **2006**, *39*, 8440–8450. [CrossRef]

11. Tricot, M. Chain flexibility parameter and persistence length of various poly(methacrylic acid esters). *Macromolecules* **1986**, *19*, 1268–1270. [CrossRef]

12. Li, Y.; Zhang, M.; Mao, M.; Turner, S.R.; Moore, R.B.; Mourey, T.H.; Slater, L.A.; Hauenstein, J.R. Chain Stiffness of Stilbene Containing Alternating Copolymers by SAXS and SEC. *Macromolecules* **2012**, *45*, 1595–1601. [CrossRef]

13. Mourey, T.; Le, K.; Bryan, T.; Zheng, S.; Bennett, G. Determining persistence length by size-exclusion chromatography. *Polymer* **2005**, *46*, 9033–9042. [CrossRef]

14. Duhamel, J. New Insights in the Study of Pyrene Excimer Fluorescence to Characterize Macromolecules and their Supramolecular Assemblies in Solution. *Langmuir* **2012**, *28*, 6527–6538. [CrossRef] [PubMed]

15. Little, H.; Patel, S.; Duhamel, J. Probing the Inner Local Density of Complex Macromolecules by Pyrene Excimer Formation. *Phys. Chem. Chem. Phys.* **2023**. [CrossRef] [PubMed]

16. Mathew, A.K.; Siu, H.; Duhamel, J. A Blob Model To Study Chain Folding by Fluorescence. *Macromolecules* **1999**, *32*, 7100–7108. [CrossRef]

17. Skou, S.; Gillilan, R.E.; Ando, N. Synchrotron-based small-angle X-ray scattering of proteins in solution. *Nat. Protoc.* **2014**, *9*, 1727–1739. [CrossRef]

18. Tuukkanen, A.T.; Spilotros, A.; Svergun, D.I. Progress in small-angle scattering from biological solutions at high-brilliance synchrotrons. *IUCrJ* **2017**, *4*, 518–528. [CrossRef]

19. De Gennes, P.-G.; Gennes, P.P.-G. *Scaling Concepts in Polymer Physics*; Cornell University Press: Ithaca, NY, USA, 1979; ISBN 978-0-8014-1203-5.

20. Little, H.; Thoma, J.L.; Yeung, R.; D'sa, A.; Duhamel, J. Persistence Length and Encounter Frequency Determination from Fluorescence Studies of Pyrene-Labeled Poly(oligo(ethylene glycol) methyl ether methacrylate)s. *Macromolecules* **2023**, *56*, 3562–3573. [CrossRef]

21. Matyjaszewski, K.; Jakubowski, W.; Min, K.; Tang, W.; Huang, J.; Braunecker, W.A.; Tsarevsky, N.V. Diminishing catalyst concentration in atom transfer radical polymerization with reducing agents. *Proc. Natl. Acad. Sci. USA* **2006**, *103*, 15309–15314. [CrossRef]

22. Siu, H.; Duhamel, J. Molar Absorbance Coefficient of Pyrene Aggregates in Water Generated by a Poly(ethylene oxide) Capped at a Single End with Pyrene. *J. Phys. Chem. B* **2012**, *116*, 1226–1233. [CrossRef]

23. Press, W.H.; Flannery, B.P.; Teukolsky, S.A.; Vetterling, W.T. *Numerical Recipes. The Art of Scientific Computing (Fortran Version)*; Cambridge University Press: Cambridge, UK, 1992; p. 82.

24. Kratky, O.; Porod, G. Röntgenuntersuchung Gelöster Fadenmoleküle. *Recl. Trav. Chim. Pays-Bas.* **1949**, *68*, 1106–1122. [CrossRef]

25. Rathgeber, S.; Pakula, T.; Wilk, A.; Matyjaszewski, K.; Beers, K.L. On the shape of bottle-brush macromolecules: Systematic variation of architectural parameters. *J. Chem. Phys.* **2005**, *122*, 124904. [CrossRef]

26. Terao, K.; Takeo, Y.; Tazaki, M.; Nakamura, Y.; Norisuye, T. Polymacromonomer Consisting of Polystyrene. Light Scattering Characterization in Cyclohexane. *Polym. J.* **1999**, *31*, 193–198. [CrossRef]

27. Farhangi, S.; Duhamel, J. Probing Side Chain Dynamics of Branched Macromolecules by Pyrene Excimer Fluorescence. *Macromolecules* **2015**, *49*, 353–361. [CrossRef]

28. Rathgeber, S.; Pakula, T.; Wilk, A.; Matyjaszewski, K.; Lee, H.-L.; Beers, K. Bottle-brush macromolecules in solution: Comparison between results obtained from scattering experiments and computer simulations. *Polymer* **2006**, *47*, 7318–7327. [CrossRef]

29. Rumble, J.R. Viscosity of Liquids. In *CRC Handbook of Chemistry and Physics*, 101st ed.; Electronic, Ed.; CRC Press: Boca Raton, FL, USA; Taylor & Francis: Oxford, UK, 1978; pp. 239–242.

30. Lakowicz, J.R. *Principles of Fluorescence*, 3rd ed.; Springer: New York, NY, USA, 2006; pp. 56, 284–287.

31. Thoma, J.; McNelles, S.A.; Adronov, A.; Duhamel, J. Direct Measure of the Local Concentration of Pyrenyl Groups in Pyrene-Labeled Dendrons Derived from the Rate of Fluorescence Collisional Quenching. *Polymers* **2020**, *12*, 2919. [CrossRef] [PubMed]

32. Patel, S.; Duhamel, J. Macromolecular Conformation of Low-Generation PAMAM Dendrimers Probed by Pyrene Excimer Formation. *Macromolecules* **2023**, *56*, 4012–4021. [CrossRef]

33. Fredrickson, G.H. Surfactant-induced lyotropic behavior of flexible polymer solutions. *Macromolecules* **1993**, *26*, 2825–2831. [CrossRef]

34. Qi, H.; Liu, X.; Henn, D.M.; Mei, S.; Staub, M.C.; Zhao, B.; Li, C.Y. Breaking translational symmetry via polymer chain overcrowding in molecular bottlebrush crystallization. *Nat. Commun.* **2020**, *11*, 2152. [CrossRef]